

# THE INFLUENCE OF PROCESSING PARAMETERS ON THE TRANSITION ZONE FOR BLENDED MATERIAL 3D PRINTING

James C. Brackett<sup>1</sup>, Dakota Cauthen<sup>1</sup>, Tyler C. Smith<sup>1</sup>, Vlastimil Kunc<sup>2</sup>, Chad Duty<sup>1,2</sup>

<sup>1</sup>University of Tennessee – Knoxville  
1512 Middle Drive  
Knoxville TN 37916

<sup>2</sup>Manufacturing Demonstration Facility  
Oak Ridge National Laboratory  
Oak Ridge, TN

## ABSTRACT

The use of Multiple Materials (MM) in Additive Manufacturing (AM) is increasingly important for expanding the range of applications in the manufacturing industry, particularly for large-format processes. Typically, polymer-based AM incorporates MM transitions through discrete interfaces between layers. This arrangement significantly increases the occurrence of layer delamination failures due to decreased bonding between dissimilar polymers. Elimination of discrete material interfaces by continuously transitioning from Material A to B provides a possible solution. Such continuous gradients could be used to create functionally graded structures that take full advantage of AM's capability to deliberately impart site-specific properties. Cincinnati's Big Area Additive Manufacturing (BAAM) system at Oak Ridge National Lab has been equipped with a dual-hopper system that enables in-situ material switching specifically intended for functionally graded and MM printing. The resulting material transition exhibits varied behavior based on printing conditions, which can have an impact on part design and resulting mechanical properties. In this work, the transition zone is characterized as a function of the printing screw speed (related to volumetric flow) and the screw geometry.

Corresponding author: James Brackett, [jbracke4@vols.utk.edu](mailto:jbracke4@vols.utk.edu)

## 1. INTRODUCTION

The recent rise of numerous Additive Manufacturing (AM) techniques has enabled precise production of complex geometries with minimal waste. Specialization of AM systems has made processing of polymers, metals, and ceramics possible. Depending on the system in use, material feedstock can appear in a variety of forms, from solid wires to fine powders.

*This manuscript has been authored in part by UT-Battelle, LLC under Contract No. DE-AC05-00OR22725 with the U.S. Department of Energy. The United States Government retains and the publisher, by accepting the article for publication, acknowledges that the United States Government retains a non-exclusive, paid-up, irrevocable, world-wide license to publish or reproduce the published form of this manuscript, or allow others to do so, for United States Government purposes. The Department of Energy will provide public access to these results of federally sponsored research in accordance with the DOE Public Access Plan (<http://energy.gov/downloads/doe-public-access-plan>).*

*SAMPE Virtual Conference Proceedings, 2020. Society for the Advancement of Material and Process Engineering – North America.*

## **1.1 Multiple Material Additive Manufacturing**

A recent area of focus has been the implementation of Multiple Materials (MM) in a single AM system. Multiple Material Additive Manufacturing (MMAM) systems use more than one material, not including pre-mixing or pre-compositing, and does not rely on non-AM post-processing treatments to complete the product [1]. Exploring the full potential of MMAM systems is crucial to continuing the expansion of AM in general. For example, appropriate design considerations can be applied to a MMAM system to create Functionally Graded Materials (FGM). As defined by Loh et. al., an FGM seeks to fulfil a functional purpose through a defined variation of density (single material) or composition (MM) in one or more directions [2]. An FGM appears in either a stepwise or continuous form. The stepwise sub-category is characterized by multiple regions of differing composition or microstructure that are separated by discrete boundaries and arranged to form an overarching gradient. Alternatively, a continuous FGM forgoes discrete interfaces for a controlled, smooth gradient in microstructure or composition that fulfills a functional requirement [3].

## **1.2 Multi-Material Additive Manufacturing**

### ***1.2.1 Multi-Material Structures***

MMAM systems have been used to create a variety of structures, but a common theme is the struggle to bond dissimilar materials in-situ. Even a small difference, such as the presence of matrix reinforcement or an additive to induce color change, between two otherwise identical polymer matrices can cause issues. Roger and Krawczak investigated the bonding of a carbon black-filled Acrylonitrile Butadiene Styrene (ABS) with virgin ABS in three different printing orientations using a multi-nozzle Fused Deposition Modelling (FDM) printer. Although utilizing an interpenetrating pattern to prevent the interface from occupying a single plane improved tensile strength compared to a typical wall-like interface, it still failed to achieve a tensile strength comparable to the weakest constituent [4]. Kim et. al. conducted a similar study on material interfaces using ABS and Poly-Lactic Acid (PLA) with a dual-nozzle FDM system. It focused on the number of interfaces, their location, and the volume percent of each material. Increasing PLA content by increasing the size of its designated region provided no significant improvement, indicating that the interface between the two dissimilar materials were hampering the print's tensile strength. Fractures along interfaces and voids observed prior to testing supported this conclusion. Fixing the ABS:PLA ratio at 1:1, using multiple interfaces in the build and z-directions highlighted the importance of structural arrangement and showed that boundaries in the z-direction significantly improved tensile strength while the number of interfaces had a minimal effect. Additionally, the interfaces parallel to build direction consistently resulted in voids vulnerable to delamination [5]. A similar MM study that also used a dual-nozzle FDM printer took a different approach. With a specialized nozzle that allowed deposition of material into voids left in previous layers, the "z-pinning" method improved interfacial strength of a PLA-Nylon MM print in tensile testing. Furthermore, the failure mode shifted from delamination to failure of the mechanical interlocking created by extruding the PLA "pins" into the voids left in the previously deposited layers of Nylon [6].

Another study using a multi-nozzle Fused Filament Fabrication (FFF) printer examined an ABS/PLA face sheet/core sandwich structure. Comparing the three-point bend performance of single-material PLA sandwiches to the dual material prints initially exhibited a significantly lower

modulus due to delamination. However, printing a PLA sandwich with the two separate nozzles needed for dual-material FFF printing resulted in comparable mechanical properties to the ABS/PLA sandwich. For MMAM, this development implicates excessive cooling of previous layers may also play a role in interface vulnerability in addition to bonding of dissimilar materials [7]. Vu et. al. also investigated interface bonding in dual-material sandwich panels using an inkjet printing system. T-Peel testing showed fractures favored the material interfaces, but fracture resistance improved when printing the material interfaces perpendicular to build direction, similar to Kim et al. [8]. Additionally, Vu et. al. also observed greater fracture toughness in specimens printed with a stepwise FGM core compared to its single-material counterpart [9]. While there is an overlap between MM and FGM structures, a distinction and separate discussion of the effects of FGM design is worthwhile.

### ***1.2.2 Stepwise Functionally Graded Materials***

Other studies have been focused entirely on using stepwise FGM design in conjunction with MMAM to improve performance in MM structures. In one study, a stepwise FGM structure was created using nine different materials with elastic moduli varying from 1 MPa to 1 GPa to achieve a mix of flexibility and rigidity. Applying this technique to a custom robot shell resulted in the increased survivability observed in a flexible version while still maintaining its shape and function like the rigid version [10]. In other MM systems, software issues in placing more than one material in the same layer can limit their functionality. This issue is commonly found in boundary-representation approaches, so an investigation into printing FGM structures sought to develop a volumetric method. The resulting software successfully demonstrated MM placement suitable for stepwise FGM's by creating regions within layers of both controlled porosity and different materials [11]. However, FGM production has not been limited to small-scale systems. For instance, Cincinnati's Big Area Additive Manufacturing (BAAM) system can use its screw-based extrusion to blend pelletized feedstock, allowing for customizable control of stepwise gradients across a part. Sudbury et al. explored this potential through printing of modified sandwich structures. The study utilized a carbon-fiber filled ABS and unfilled ABS to explore the weight and cost savings of a stepwise FGM compared to a single-material print. The gradients successfully reduced both cost and weight of the final structure, highlighting some of the possible benefits of incorporating FGM into AM [12]. However, this approach limited the possible gradients to the z-direction and requires a single composition for each layer.

### **1.3 Exploration of Continuous Functionally Graded Materials**

Addressing BAAM's initial limitations is necessary to fully capitalize on its MMAM potential. The extrusion-based process benefits from both its feedstock type (pellets) and extrusion mechanism (screw). The pelletized feedstock can be easily mixed and does not suffer from any continuity issues that would require a stoppage of the printing process. Similarly, screw-based extrusion ensures that the feedstock mixes inside the barrel to form a singular bead, again allowing for continuation of a print regardless of feedstock changes. A new configuration was developed to harness these unique advantages and applied to the BAAM-B system at Oak Ridge National Lab (ORNL).

### ***1.3.1 A Dual-Hopper System for Multi-Material Additive Manufacturing***

An innovative dual-hopper system was constructed and attached to BAAM-B's print-head to enable MM feeding and in-situ material changes. Shown in Figure 1, each hopper connects to a different feedstock source. Only one hopper feeds into the barrel at a time, but a simple manual or coded command will switch them, changing material on-the-fly without interrupting the print in any way. The switch is completed by a simple rocker mechanism that forces the currently feeding hopper closed while pushing the secondary hopper into position over the barrel. The BAAM-B's redesigned material feeding system allows for printing of MM, stepwise FGM, and continuous FGM structures.



Figure 1. Image of the dual-hopper attachment and feeding tubes for BAAM-B.

### ***1.3.2 Continuous Transitions***

With the dual-hopper system, the BAAM inherently creates a blended region, termed the transition zone. shortly after the switch caused by mixing of the pellets both above the barrel and in the melt. Thus, it can incorporate a continuous material transition in its prints by strategically placing hopper switches at pre-specified points. However, this requires knowing the characteristics of the material transition induced by the dual-hopper and extrusion screw. Describing the transition zone mathematically with a “shape function” would aid in defining design constraints and predicting mechanical properties around the zone. For this, the initial step is constructing a “shape curve” of the transition process. In general, this requires tracking the material composition, i.e. % Material A, over an arbitrary distance until the composition is 100 % Material B. Figure 2 shows a few possibilities. An “ideal” scenario could be represented by a weighted mean or rule of mixtures as

is commonly done when predicting the material properties of simple mixtures [13]. However, this approach expects an even, consistent mixture. The abrupt change introduced by a hopper switch, in conjunction with screw-driven mixing, will likely result in a non-linear transition zone., which is represented by the dotted-lines in Figure 2. Considering the variety of factors present in AM and specifically on the BAAM, multiple factors could influence the final shape curve's characteristics. Each observed shape curve is expected to be unique to the material pair in question just as each composite material exhibits a different range of properties even if only one constituent is altered. For example, a material's rheological properties and reinforcement type and quantity have a large influence on how it will mix, making the three variables a likely source of change in the shape curve. From a system contributions perspective, the BAAM is compatible with several different screw geometries, all of which are operated at varying rotational speeds. Additionally, the total mass output (as determined by nozzle size and coded bead dimensions) will influence the observed distance or time to complete the transition zone. Each of these material and instrument parameters could lead to a change in the transition zone's length or shape.

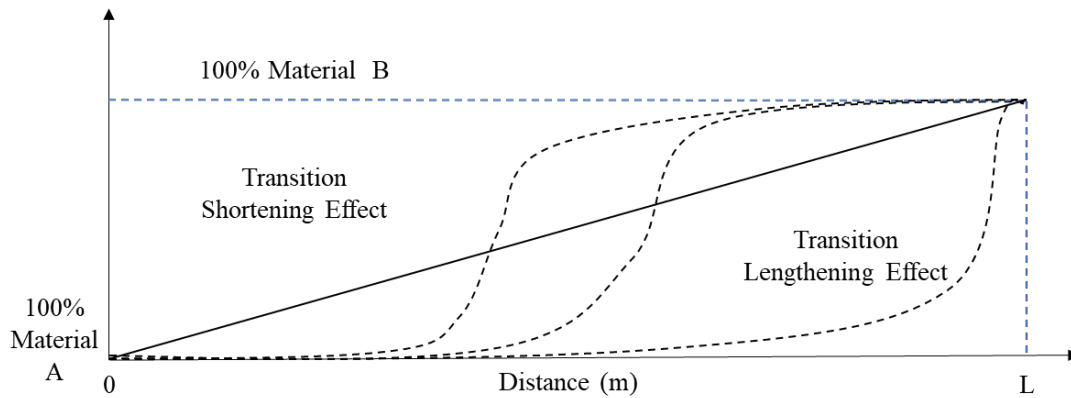


Figure 2. An illustration of a few possible transition behaviors. The solid line indicates a linear transition from Material A to Material B, while the dotted lines demonstrate some of the possibilities for the more likely non-linear behavior.

### 1.3.3 Continuous Transition Examples

A few previous studies have demonstrated the BAAM's capability for continuous transitions. The first examined a glass fiber-filled ABS to carbon fiber-filled ABS using manual feeding at 100 Rotations Per Minute (RPM). Obtained using Thermogravimetric Analysis, the fiber content at selected locations was plotted to develop an initial shape function, which indicated the system required a travel distance of 1.5 m (15 ft) to achieve steady-state conditions [14]. In a follow-up study, Sudbury et. al. examined the effect of screw speed on the transition time from a neat ABS to carbon fiber-filled ABS. With transition times of 52 s at 100 RPM and 5.85 s at 400 RPM, increasing the screw's rotational speed by 400% disproportionately reduced the transition time by almost 90% [15]. This indicates that the screw speed may influence the travel distance required for a material transition to occur. Another study examined the in-situ capability and process repeatability of the dual-hopper modification. It found a consistent and repeatable transition behavior when printing the same object multiple times and provided evidence that the transition zone maintains a consistent trend toward the secondary material with no deviation from surrounding areas. Furthermore, closer inspection revealed that the direction of transition also

functions as an influencing parameter. In this case, transitioning from ABS to a carbon fiber-filled ABS completed earlier than its reverse in addition to having a difference in initiation and transition zone lengths [16]. Clearly, the BAAM is more than capable of producing continuous FGM structures, but the finer aspects to transition behavior still need to be characterized.

#### **1.4 Importance of BAAM System Parameters**

The previous work has focused on understanding the general process of the material transitions produced when using the modified BAAM's dual-hopper system. To further understand the contributing factors, an analysis of the system's possible affects is necessary. RPM is commonly changed from one print to another, so understanding its contribution will inform any future prints and guide print design. Similarly, the extrusion screw's geometry could alter the transition behavior and prove to be a valuable tool in controlling the shape function. As such, the effect of each is critical for accurately implementing site-specific properties via MM and FMG structures in large-scale MMAM with the BAAM. While a change in transition time was observed in [15] at different RPM's, a complete picture obtained by tracking both distance and time allows for a direct comparison to the previous work and a discussion on the print space required for each. The influence of the screw's geometry is examined by comparing transitions produced by a "non-mixing" and "mixing" screw. Upon completion, this work will be able to predict the effects of altering RPM and screw geometry.

## **2. EXPERIMENTATION**

### **2.1 Sample Production**

The pelletized feedstocks supplied by Techmer Engineered Solutions were a neat ABS (HIFILL ABS 1512 3DP) and a 20 wt % carbon fiber-filled ABS (ELECTRAFIL ABS 1501 3DP). Prior to printing with the dual-hopper BAAM, each material was dried at 80 °C for at least four hours. A single, continuous bead 5.97 m (235 in) long was printed as shown in Figure 3. Each print used a nozzle of 10.16 mm (0.4 in), a bead height of 5.08 mm (0.2 in), and a bead width of 13.97 mm (0.55 in). The rotational speed of the screw was set to either 100 or 300 RPM, and a print was completed at each speed, once with a "mixing" and once with a "non-mixing" screw geometry. The travel speeds were 4.3 cm/s (1.7 in/s) and 10.7 cm/s (4.2 in/s) for the 100 RPM and 300 RPM prints, respectively. Thermal conditions were maintained at a 100 °C bed temperature and 250 °C at the melt. With these conditions, the impact of both rotational speed and differing screw geometries on the total length and general shape of the transition curve. After printing, the sample beads were sectioned with a bandsaw and labeled for easy tracking of distance and time from the point the hopper switch occurred. As shown by [16], an 8.4 mm sample was consistently representative of the surrounding 25.4 mm. Maintaining this approach, an Isomet 1000 Precision Saw extracted single 8.4 mm samples from each location of interest for characterization.



Figure 3. A 100 RPM sample printed with BAAM-B's dual-hopper.

## 2.2 Characterization Method

Charting the transition from neat to carbon fiber-filled ABS requires a means of tracking material composition at any given point in the bead. For this material pair, carbon fiber content by weight can be used as a reliable indicator. To obtain a standard residual value for each material, three batches of both ABS and CF/ABS as-provided pellets were submitted to characterization. The average resulting fiber content of the CF/ABS pellets will be used as a baseline. All mass measurements were conducted with a RADWAG AS 220.R2 analytical balance with a 0.1 mg accuracy.

ASTM D3171-15 provides several procedures for constituent content analysis, including some that utilize an acid to attack the matrix and hydrogen peroxide to accelerate the reaction [17]. Using this approach as inspiration, a custom method for digesting the polymer matrix was developed. Ultrasonic Assisted Acid Digestion (UAAD) replaces hydrogen peroxide with a sonicator bath that enables digestion of the ABS matrix with simple acetone. Prior to UAAD, samples are dried at 80 °C and their dry mass recorded. A Lab Safety Supply glass microfiber filter with 47 mm diameter and 1.5  $\mu\text{m}$  pores, also dried and weighed, is assigned to each sample. For testing, specimens are placed in a borosilicate glass tube or vial and submerged in HPLC Acetone of  $\geq 99.5\%$  purity. The vials are placed in the sonicator bath for thirty minutes. Upon complete dissolution of the matrix, any remaining fibers are separated from the solution using the previously mentioned filters in a vacuum-assisted filtration set-up. The filter is extracted from the apparatus and then dried at 80 °C overnight before final mass measurements.

The dry mass of the fibers is compared to the original dry mass of the sample to calculate the fiber content by weight, but it also borrows from ASTM D3171-15 by including a ratio that compensates for any polymer left behind. Originally intended as a “carbonization ratio” for procedures using combustion, this study will use an average Dissolution Ratio,  $DR$ , obtained from the neat ABS control samples to adjust for the typical amount of polymer captured in the filtering process. In Equation [1],  $m_{cr}$  is the measured mass of the pan and filter after UAAD,  $m_c$  is the measured mass of pan and filter prior to UAAD, and  $m_i$  is the dry mass of the specimen. Equation [2] shows how the  $DR$  is used in calculating the fiber content. Again,  $M_i$  is the mass of the specimen,  $M_{cr}$  is the mass of the pan and filter after UAAD, and  $M_c$  is the mass of the pan and filter prior to UAAD. Since this process is originally intended for analysis of polymer composites, measurements of neat or near-neat samples have the potential to experience greater degradation. Due to this slight variability, non-reinforced samples could return a negative fiber content up to -1.0 wt %.

$$DR = \frac{m_{cr} - m_c}{m_i} \quad [1]$$

$$\text{Fiber \%} = \left( \frac{M_i - \left( \frac{M_i - (M_{cr} - M_c)}{1 - DR} \right)}{M_i} \right) \times 100 \% \quad [2]$$

### 2.3 Shape-curve construction

To examine the differences in transition behavior, the fiber content measurements for each sample set are plotted as a function of distance traveled from when the hopper switch was initiated. Each transition curve will begin with a Purge Zone, proceed to a Transition Zone, and eventually reach a Steady-State Zone. Assessing any variance between the curves in each zone’s initiation, length, and termination will inform future work and provide design tools for controlling material transitions in full-scale FGM and MM printing.

## 3. RESULTS

### 3.1 Discussion of the Control Samples

As mentioned, unprocessed pellets were tested using UAAD to provide the necessary DR and a baseline for fiber content in the provided CF/ABS. The average  $DR$  from three batches of ABS pellets was 0.0201 and was used to calculate fiber content for all other samples. The carbon fiber-filled ABS pellets returned an average fiber content of 18.8 wt %, which is lower than the expected 20 wt %. Therefore, saturation will be considered as being at or above 19.0 wt % carbon fiber.

### 3.2 Parameter Influences

Utilizing UAAD, the fiber content of samples from four different parameter sets was determined. Plotting the fiber content of samples as a function of the distance from where the hopper switch was initiated provides an illustration of the transition behavior. Figure 4 demonstrates this process with the specimens from the 100 RPM printed with the mixing screw geometry. This one was chosen due to its limited variance and enables a clear designation of three different zones, as seen

in Figure 5. As shown, a print running at 100 RPM with the mixing screw has a purge zone of about 1.51 m, a transition zone of 1.72 m, and thus takes 3.23 m to reach a steady-state CF/ABS composition.

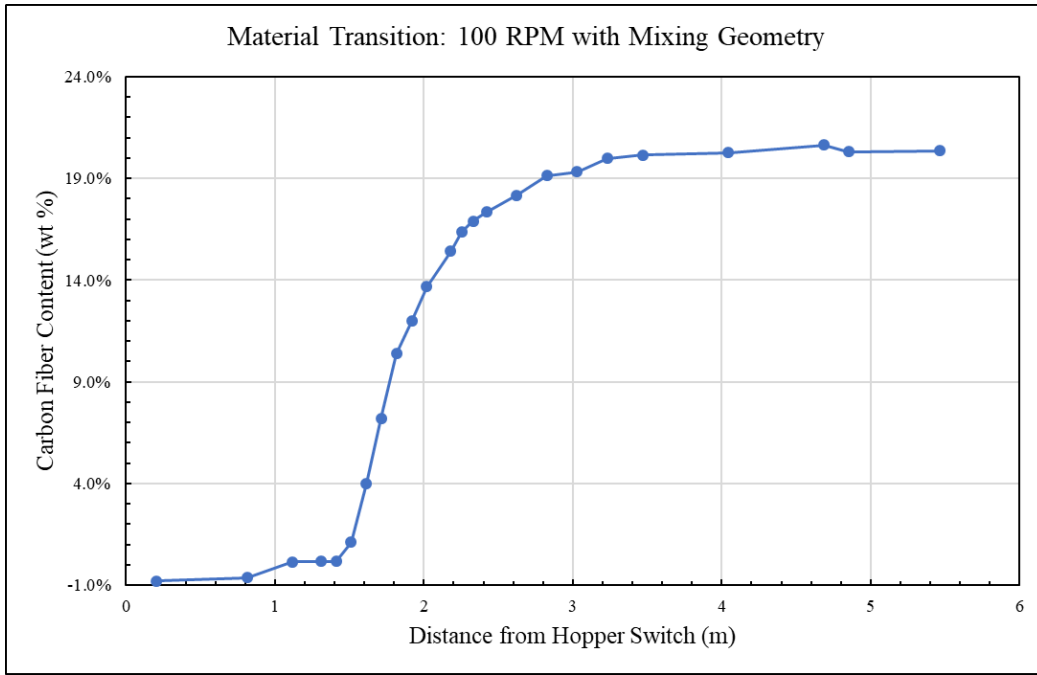


Figure 4. The shape curve for an ABS to 20 wt % CF/ABS conducted at a screw speed of 100 RPM with the mixing screw geometry.

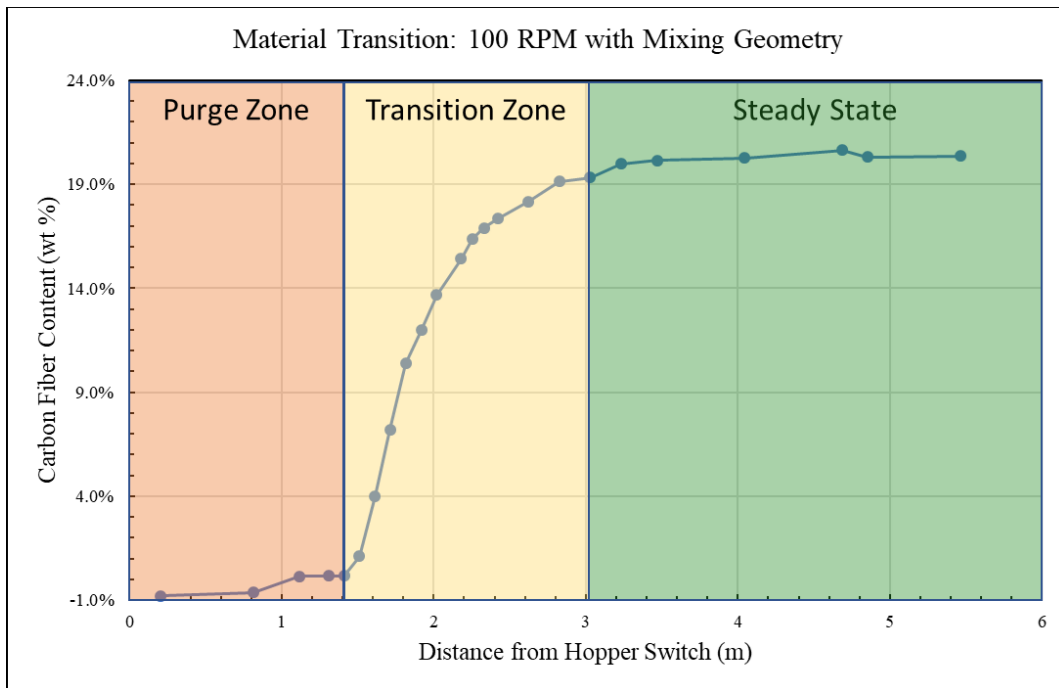


Figure 5. Definition of the three regions observed during a dual-hopper material transition.

While an in-depth microscopic analysis has not yet been completed, some preliminary images are of interest. As seen in Figure 6A and 6B, the neat ABS and CF/ABS have easily distinguishable structures. These two appearances are maintained throughout the Purge and Steady-State Zones, respectively. The Transition Zone example shown in 6C has a similar structure to the CF/ABS sample, despite only having a fiber weighting of 11.3 wt %.

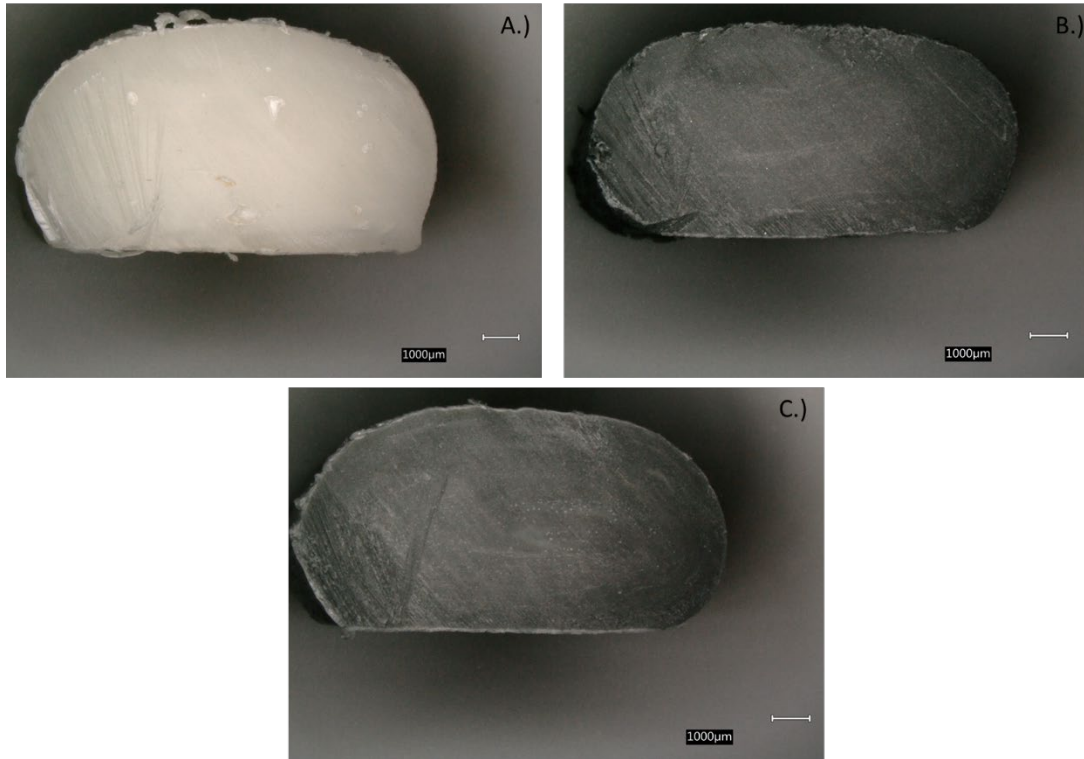


Figure 6. Microscopy of samples from the mixing screw at 300 RPM, as seen in Figure 7. A.) Purge Zone, 8<sup>th</sup> data point, b.) Steady-State Zone, 21<sup>st</sup> data point, and C.) Transition Zone, 11<sup>th</sup> Data point.

### 3.2.1 Effect of RPM

Figure 6 compares a speed of 100 RPM to 300 RPM using the mixing screw geometry. Treating the initial spike in fiber content as an anomaly, it is evident that the transition lags behind at the higher RPM, taking 2.02 m to begin compared to 1.51 m. The 300 RPM transition does exhibit a shorter transition region at 1.46 m, but the overall transition is still slightly longer at 3.48 m as a result of the extended purge zone.

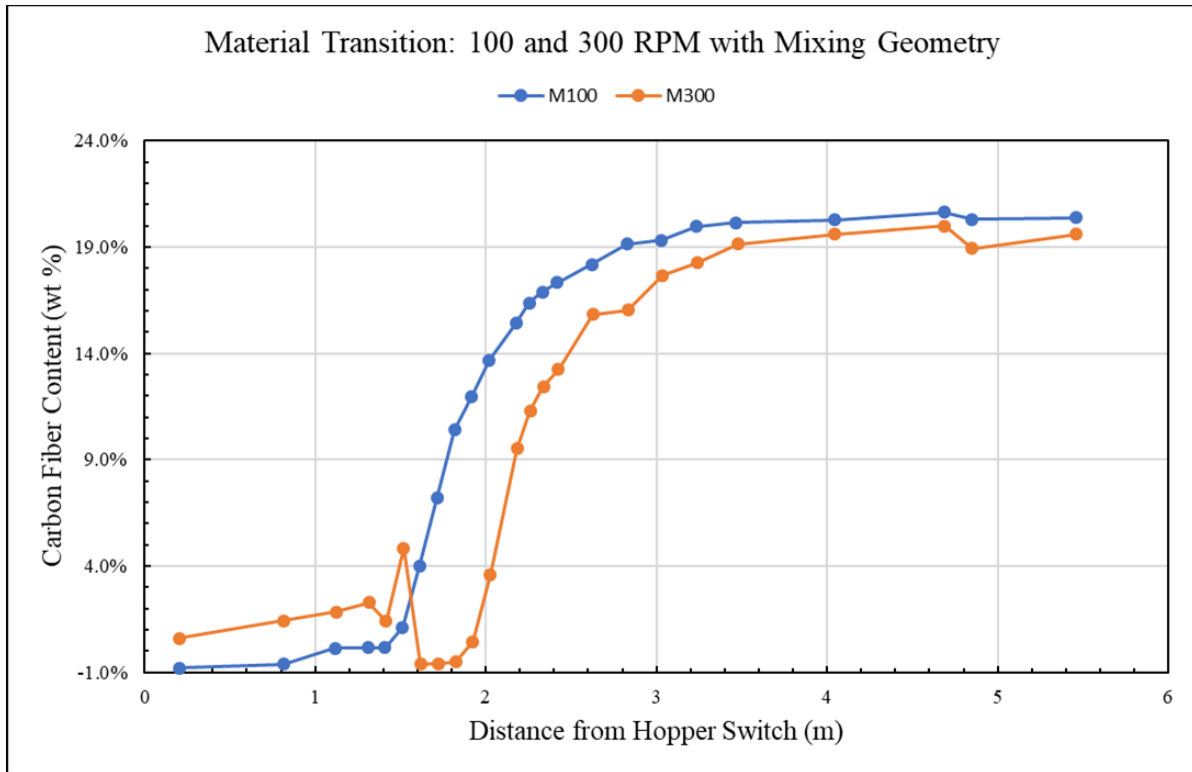


Figure 6. A comparison of the shape curves at 100 and 300 RPM. Both transitions used the mixing screw geometry.

Similarly, Figure 7 shows the same lag in transition behavior at a higher RPM, despite the change in screw geometry. Interestingly, a blip in fiber content is seen again early on in the 300 RPM transition, possibly indicating that the higher rotational speed has premature evidence of the material transition. The 100 RPM transition has a purge zone of 1.61 m compared to 1.81 m at 300 RPM, not as significant a difference as seen with the mixing screw geometry. Transition zone lengths were 1.4 m and 1.67 m. Interestingly, the distance required to reach steady state for 300 RPM was once again 3.48 m while 100 RPM was shorter at 3.01 m. Though the transitions for the non-mixing screw geometry closely resembled and tracked each other, they exhibited more variance, which caused the deviation in zone lengths. This is most evident just after 3 m where 300 RPM has a drop in fiber content. In general, the screw RPM could be valuable tool in tweaking when the transition occurs in a print and in controlling its length.

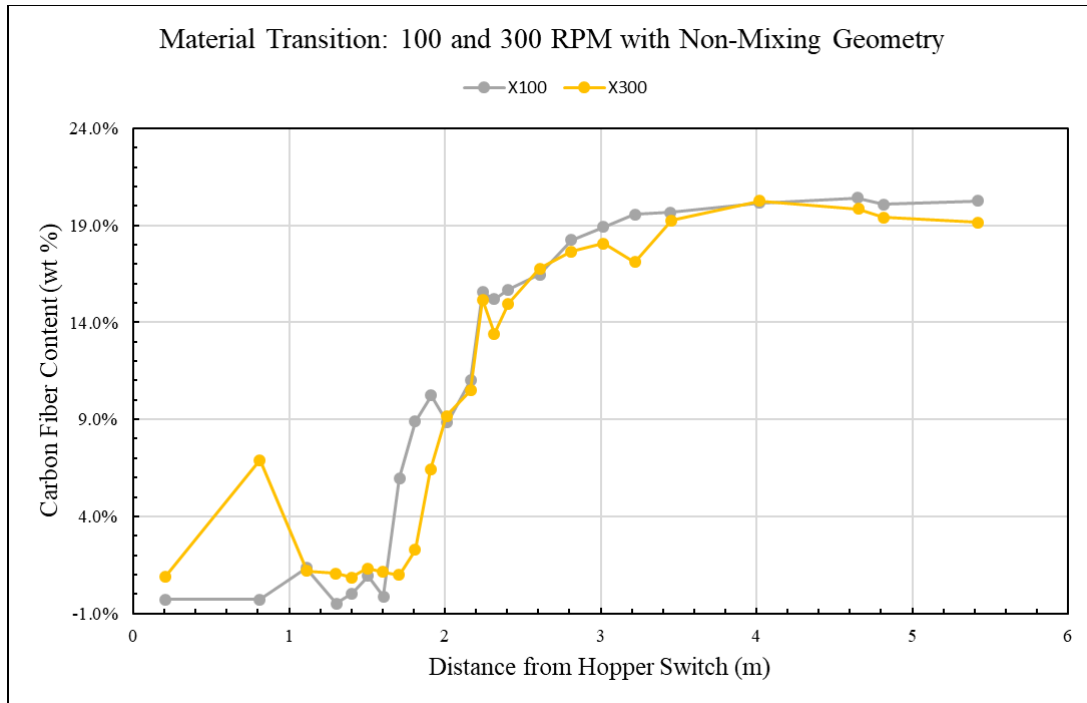


Figure 7. The shape curves obtained from specimens printed using the non-mixing screw at 100 and 300 RPM.

### 3.2.2 Effect of Screw Geometry

Combining Figures 6 and 7 provides a better opportunity to analyze screw geometry’s influence on the transition curves. As Figure 8 demonstrates, the effect is largely negligible. The 100 RPM transitions are nearly identical, with the transition zone beginning just 0.1 m later for the non-mixing screw. A possible candidate for further investigation is screw geometry at higher rotational speed. Although a difference in initiation point is observed at 300 RPM, it is again small at 0.2 m the transition completes at the same distance. The greatest effect of screw geometry appears to be in the consistency of the transition, with a larger variance appearing in the non-mixing geometry curves compared to the mixing geometry curves. Regardless, choice of screw geometry appears to have little to no impact on material transitions, allowing design considerations to focus on which screw geometry best suits the materials being processed.

As mentioned, there are a few notable outliers in the Purge Zone and noticeable variation in the non-mixing curves. Initial UAAD testing exhibited a standard deviation of only 0.08 wt %, and the CF/ABS pellets had a deviation of 0.29 wt %. Considering similar processes have reported testing error to be  $\leq \pm 1$  wt % [18], applying the same rule is prudent for UAAD. However, the anomalies observed are greater than the accepted error. Thus, their source could be attributed to sample variation or operator error, or it may indicate that the measurement process is still in need of some refinement. Either way, further analysis will be needed to accurately address the issue. Regardless, the data still supplies easily observable trends useful for characterizing the transition behavior.

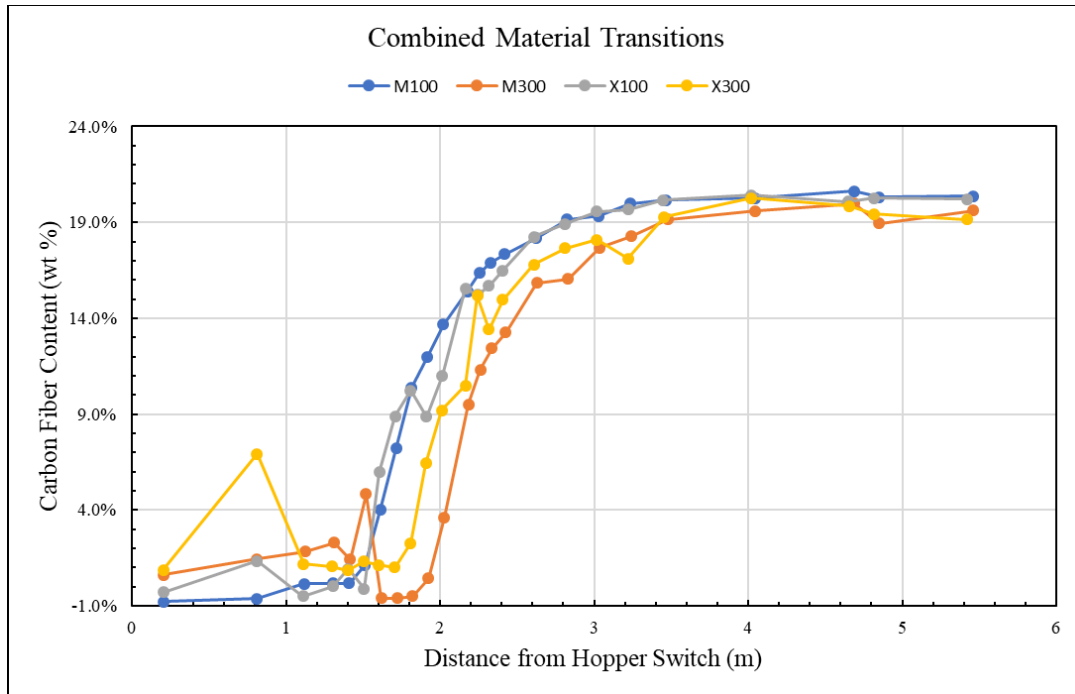


Figure 8. A combined plot of all four characterized transitions. All four transitions exhibit a similar pattern, with the slight alterations caused by parameters visible when side-by-side.

#### 4. CONCLUSIONS

UAAD successfully characterized the fiber content by wt % of a multitude of samples. From this data, four distinct shape curves for an ABS to CF/ABS transition were constructed and compared. The rotational speed of the screw in a BAAM system slightly increases the distance required to reach steady state CF/ABS extrusion. This was true regardless of the screw geometry. Furthermore, the presence of a static mixer in a screw’s geometrical profile had a negligible effect, as evidenced by the resulting shape curves of different screw geometries at the same RPM generally overlapping.

These effects further inform design for MMAM using BAAM-B’s dual-hopper system, especially when printing FGM structures. Given that the screw geometry had no observable influence on the shape curve, a screw’s geometry can be chosen solely based on the characteristics needed for the materials involved. The screw RPM, however, had a noticeable effect, with a higher RPM delaying completion of the transition. Thus, screw RPM can be used as a tool to tweak the transition profile for a material pair to better suit the design’s requirements.

#### 5. ACKNOWLEDGEMENTS

Research sponsored by the U.S. Department of Energy, Office of Energy Efficiency and Renewable Energy, Industrial Technologies Program, under contract DE-AC05-00OR22725 with UT-Battelle, LLC. Thanks to Techmer Engineered Solutions for providing material for this study. Additional thanks to Cincinnati Incorporated for providing the BAAM printing system.

## 6. REFERENCES

- [1] M. Vaezi, S. Chianrabutra, B. Mellor, and S. Yang, "Multiple material additive manufacturing – Part 1: a review," *Virtual & Physical Prototyping*, Article vol. 8, no. 1, pp. 19-50, 2013, DOI: 10.1080/17452759.2013.778175.
- [2] G. H. Loh, E. Pei, D. Harrison, and M. D. Monzón, "An overview of functionally graded additive manufacturing," *Additive Manufacturing*, vol. 23, pp. 34-44, 2018/10/01/ 2018, DOI: <https://DOI.org/10.1016/j.addma.2018.06.023>.
- [3] G. Udupa, S. S. Rao, and K. V. Gangadharan, "Functionally graded Composite materials: An overview," in *International Conference on Advances in Manufacturing and Materials Engineering*, vol. 5, S. Narendranath, M. R. Ramesh, D. Chakradhar, M. Doddamani, and S. Bontha Eds., (Procedia Materials Science. Amsterdam: Elsevier Science Bv, 2014, pp. 1291-1299.
- [4] F. Roger and P. Krawczak, *3D-printing of thermoplastic structures by FDM using heterogeneous infill and multi-materials: An integrated design-advanced manufacturing approach for factories of the future*. 2015.
- [5] H. Kim, E. Park, S. Kim, B. Park, N. Kim, and S. Lee, "Experimental Study on Mechanical Properties of Single- and Dual-material 3D Printed Products," *Procedia Manufacturing*, vol. 10, pp. 887-897, 2017/01/01/ 2017, DOI: <https://DOI.org/10.1016/j.promfg.2017.07.076>.
- [6] C. Duty, J. Condon, T. Smith, A. Lambert, S. Kim, and V. Kunc, "Improving the 3D Printed Bond Strength at a Discrete Interface Between Dissimilar Materials," in *Society for the Advancement of Material and Process Engineering 2020*, Seattle, WA, May 4-7 2020, 2020.
- [7] S. Brischetto, C. Ferro, R. Torre, and P. Maggiore, "3D FDM production and mechanical behavior of polymeric sandwich specimens embedding classical and honeycomb cores," *Curved and Layered Structures*, vol. 5, pp. 80-94, 04/01 2018, DOI: 10.1515/cls-2018-0007.
- [8] I. Vu, L. Bass, N. Meisel, B. Orler, C. B. Williams, and D. A. Dillard, "Characterization of Mutli-Material Interfaces in PolyJet Additive Manufacturing," *Solid Freeform Fabrication Symposium Proceedings*, Conference Proceeding pp. 959-982, 2015.
- [9] I. Q. Vu, L. B. Bass, C. B. Williams, and D. A. Dillard, "Characterizing the effect of print orientation on interface integrity of multi-material jetting additive manufacturing," *Additive Manufacturing*, vol. 22, pp. 447-461, 2018/08/01/ 2018, DOI: <https://DOI.org/10.1016/j.addma.2018.05.036>.
- [10] N. W. Bartlett *et al.*, "A 3D-printed, functionally graded soft robot powered by combustion," (in English), *Science*, Article vol. 349, no. 6244, pp. 161-165, Jul 2015, DOI: 10.1126/science.aab0129.
- [11] B. Ezair and G. Elber, "Fabricating Functionally Graded Material Objects Using Trimmed Trivariate Volumetric Representations," *Fabrication and Sculpting Event*, Conference Proceedings 2017.
- [12] Z. Sudbury, C. Duty, and K. Vlastimil, "Expanding Material Property Space Maps with Functionally Graded Materials for Large Scale Additive Manufacturing," *Solid Freeform Fabrication Symposium Proceedings*, pp. 459-484, 2017.
- [13] M. F. Ashby \*, "Hybrids to fill holes in material property space," *Philosophical Magazine*, vol. 85, no. 26-27, pp. 3235-3257, 2005/09/11 2005, DOI: 10.1080/14786430500079892.

- [14] Z. Sudbury, C. Duty, V. Kunc, V. Kishore, C. Ajinjeru, J. Failla, and J. Lindahl, "Characterizing Material Transition for Functionally Graded Material Using Big Area Additive Manufacturing," *Solid Freeform Fabrication Symposium Proceedings*, pp. 738-747, 2016.
- [15] Z. Sudbury, C. Ajinjeru, V. Kishore, C. Duty, P. Liu, and V. Kunc, "Blending of Fiber Reinforced Materials Using Big Area Additive Manufacturing," in *Society for the Advancement of Material and Process Engineering 2017*, Seattle, WA, May 22-25 2017, 2017.
- [16] J. Brackett, Y. Yan, D. Cauthen, V. Kishore, J. Lindahl, T. Smith, H. Ning, V. Kunc, and C. Duty, "Development of Functionally Graded Material Capabilities in Large-scale Extrusion Deposition Additive Manufacturing," *Solid Freeform Fabrication Symposium Proceedings*, pp. 1793-1803, 2019.
- [17] ASTM D3171-15 "Standard Test Methods for Constituent Content of Composite Materials," ASTM International, West Conshohocken, PA, 2015, DOI: 10.1520/D3171-15, [www.astm.org](http://www.astm.org).
- [18] Q. Wang, H. Ning, U. Vaidya, S. Pillay, and L.-A. Nolen, "Fiber Content Measurement for Carbon Fiber-Reinforced Thermoplastic Composites Using Carbonization-In-Nitrogen Method," *Journal of Thermoplastic Composite Materials*, vol. 31, no. 1, pp. 79-90, 2018, doi: 10.1177/0892705716679481.